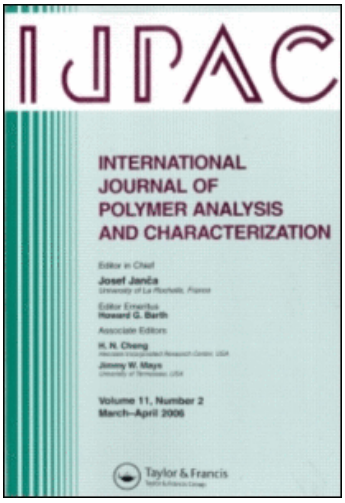

International Journal of Polymer Analysis and Characterization
Publication details, including instructions for authors and subscription information:
http://www.informaworld.com/smpp/title~content=t713646643

Comparison of On-line Single-Capillary and Bridge Capillary Viscometric Detectors for Size Exclusion Chromatography

D. P. Norwood[a]; Wayne F. Reed[a]
[a] Department of Physics, Tulane University, New Orleans, LA

To cite this Article Norwood, D. P. and Reed, Wayne F.(1997) 'Comparison of On-line Single-Capillary and Bridge Capillary Viscometric Detectors for Size Exclusion Chromatography', International Journal of Polymer Analysis and Characterization, 4: 2, 99 — 132
To link to this Article: DOI: 10.1080/10236669708033941
URL: http://dx.doi.org/10.1080/10236669708033941

Int. J. Polym. Anal. Charact.
1997 Vol. 4, pp. 99–132
Reprints available directly from the publisher
Photocopying permitted by license only

Comparison of On-line Single-Capillary and Bridge Capillary Viscometric Detectors for Size Exclusion Chromatography

D. P. NORWOOD and WAYNE F. REED*

Department of Physics, Tulane University, New Orleans, LA, 70118

(Received 22 November 1996; Revised 15 April 1997)

A systematic and thorough comparison is made of a laboratory-built single-capillary viscometer and a bridge viscometer, integrated together into a size exclusion chromatography (SEC) apparatus incorporating a multi-angle laser light scattering (MALLS) photometer and a differential refractometer. It is demonstrated that proper choice of the SEC pump is crucial to realize the potential accuracy of either viscometer design. Random measurement error contributes an order of magnitude greater error in the single-capillary viscometer than in the bridge viscometer, and thus the bridge viscometer gives significantly greater precision in any one measurement. Other sources of error, such as calibration error and stochastic variation from one run to the next, however, reduce the bridge viscometer's greater precision to only about a factor of two greater than the single-capillary design. Two advantages compensating for the laboratory-built single-capillary viscometer's decreased precision are its compactness and its significantly lower cost. By the use of variety of polymers (hyaluronate, poly(vinyl pyrrolidone) and dextran), estimates of scaling laws for both root-mean-square radius of gyration and reduced viscosity are made, and their accuracies and sources of error assessed.

Keywords: Size exclusion chromatography, viscometry, light scattering

INTRODUCTION

The measurement of specific viscosity is a well-established technique in the field of polymer characterization. These measurements provide valuable information regarding polymer characteristics, a few examples of

* Corresponding author.

which are molecular weight, branching character, chain conformation and polymer-solvent interactions.[1–9] The utility of the viscometric technique is enhanced by coupling viscometry with size exclusion chromatography. This permits a quick and relatively simple measurement of the behavior of polymer viscosity as a function of polymer molecular weight, exactly the terms in which many theories of polymer viscosity are cast.[10,11] Two common viscometers used on-line in size exclusion chromatography, both based on Poiseuille's equation, are the single-capillary viscometer[12] and the bridge viscometer.[13] The former uses the change in pressure drop along a single-capillary to measure viscosity, whereas the latter measures the imbalance in flow, caused by a viscosity difference, through the various capillaries arranged in a "Wheatstone bridge" configuration. It is the purpose of this paper to systematically compare the performance of these two types of viscometer in conjunction with SEC, and describe the principal advantages and disadvantages of each. These viscometers can also be used with other separation techniques, such as field flow fractionation.[14–16] (FFF) and capillary hydrodynamic fractionation[17] (CHDF).

EXPERIMENTAL

Apparatus

The size exclusion chromatography (SEC) system consisted of an ISCO 2350 HPLC pump (Isco Inc., Lincoln, NE), which was later replaced by a Hewlett Packard Series 1100 isocratic pump (Hewlett Packard, Wilmington, DE), two Shodex OHPak columns in series (Showa Denko America, Inc., New York, NY), a Wyatt Technology Dawn-F laser photometer (Wyatt Technology Corporation, Santa Barbara, CA), an Erma ERC-7522 refractive index detector (Erma CR. Inc., Tokyo, Japan), a single-capillary viscometer built around a Validyne DP15-28 pressure transducer (Validyne Engineering Corp., Northridge, CA), and a Viscotek Model 100 differential viscometer (Viscotek, Porter, TX).

The two pumps were both standard analytical chromatographic pumps, and had the same nominal specifications. However, a crucial difference in the performance is the pulsation produced by the pumping action. While specifications were similar (and in both cases, performance was better than specified), actual performance was quite different and this had a dramatic

effect on the performance of both viscometers, but particularly for the single-capillary design. This will be discussed further below. The pumps were operated at a specific flow rate, either 0.4, 0.8 or 1.2 mL/min., which was verified by measuring the volume eluted in a given time period.

The Shodex columns were the SB 805 HQ, followed by the SB 806 HQ. The column packing material was poly(hydroxymethyl methacrylate). The particle size in each case was 10 ± 2 μm, while the pore size was 100 nm for the 805 and 200 nm for the 806.

Immediately after the columns was a Wyatt Technology Dawn-F multi-angle laser light scattering detector (MALLS.)[18] This detector unambiguously provides the mass and radius of gyration of the eluting polymer, thus obviating the need for column calibration. The Dawn-F was fitted with a flow cell for use in the SEC apparatus. The Dawn F incorporates a vertically polarized 5 mW helium-neon laser, and simultaneously detects laser scattering at 15 angles from 21.5° to 158.5°. Measurements at these fifteen angles, plus the refractive index measurement, are sent to an IBM 486 computer by way of a DT2801-A 12 bit analog to digital conversion board, as per the standard commercial configuration of the Dawn-F.

Following the photometer was an ERC-7512 deflection-type differential refractometer. Given the increment of refractive index, dn/dc, this reading (also supplied to the computer via the DT2801-A) provides an independent measure of the concentration eluting at each sampled point, without the need to assume that all material is eluted. The concentration, c_i, at a given elution point, i, is given by

$$c_i = \frac{V_{RI,i}.CF}{\partial n/\partial c} \tag{1}$$

where $V_{RI,i}$ is the voltage reading from the refractometer for elution point i, dn/dc is the specific refractive index increment for the polymer, and CF is the calibration factor (in Δn/volt) for the refractometer, which converts the voltage read to a refractive index change. The calibration factor was determined by injecting a number of NaCl solutions, whose concentrations varied from 5 to 25 mM, then using the voltage measured by the refractometer, and the known index change for each salt solution, which at a wavelength of 633 nm and a temperature of 25°C, is given by[19] $\Delta = 1.766 \cdot 10^{-3}$[NaCl] for [NaCl] in g per 100 g of H_2O. The calibration factor, which had a standard deviation of about 0.85%, was about 11% higher than the manufacturer's specification. This indicates some decline in the refractometer's

performance over time, and reinforces the need to carefully calibrate the refractometer in order to obtain accurate results for both molecular weights and intrinsic viscosities.

The single-capillary (SC) viscometer was built around the Validyne DP15-28 variable reluctance differential pressure transducer. The two terminals of the transducer were attached to "T" connectors, between which was a 20-cm length of 0.020 in ($5.08 \cdot 10^{-4}$ m) diameter capillary tubing. For a given flow rate, the viscosity of the eluting fluid is related to the pressure drop across the capillary through Poiseuille's equation:

$$\eta = \frac{\pi R^4 P}{8LQ} \tag{2}$$

where R is the inner radius of the capillary tube, P is the pressure drop of the fluid along the capillary, L is the length of the capillary, and Q is the volume flow rate. When, as is commonly done, using cgs units (P in dynes-cm^{-2}, Q in cm^3-s^{-1}, and R and L in cm), the viscosity is in poise (g-cm^{-1}-s^{-1}). For SI units (P in pascals, Q in m^3-s^{-1}, and R and L in m), the viscosity is in Pa-s. Tubing of the specified length and diameter has a volume (and thus a resolution) of about 40 μL, and an average shear rate, given by

$$\dot{\gamma}_{AVE} = \frac{8Q}{3\pi R^3} \tag{3}$$

of 345, 690, and 1036 s^{-1} at a flow rate of 0.4, 0.8, and 1.2 mL/min, respectively. Peak shear rates, occurring near the walls of the capillary, are 50% higher. These high shear rates are intrinsic to on-line capillary viscometry, and must be considered in any attempt to interpret the viscosity measured, particularly for materials which evidence shear dependent viscosity.[20] The DP15-28 transducer was connected to a Model CD12 carrier demodulator which provided a −10 V to +10 V signal proportional to the pressure difference across the capillary. This was read by a separate A/D board (model DT2805/5716) on the same computer, which was dedicated to the two viscometers.

The bridge viscometer, which is also based on Poiseuille's equation, is a Viscotek Model 100 differential viscometer (Viscotek, Houston, TX) which incorporates four capillaries of length 24 in. and inner diameter of 0.010 in. ($2.54 \cdot 10^{-4}$ m), arranged in a "Wheatstone bridge" configuration. With the "Wheatstone bridge" design, viscometer data depend on ratios of flow rates through the various arms, rather than absolute flow rates, making

the bridge viscometer less susceptible (although not immune) to variations in overall flow rate and pressure. Each capillary of the bridge viscometer has a dead volume of about 50 μL and an average shear rate of 2763, 5525, and 8288 s^{-1}, at a flow rate of 0.4, 0.8, and 1.2 mL/min, respectively. Additionally, the bridge viscometer depends on a holdup reservoir which holds back half of the injected sample for 30 mL of elution. This must be considered when interpreting the readings on instruments downstream of the Viscotek. We found it best to place the Viscotek at the end of the train of instruments. All detectors were arranged serially, and the order of detectors after the columns was: MALLS, refractometer, single-capillary viscometer, and bridge viscometer. Software was written to capture the multiple signals via the two A/D boards and to analyze the results.

Materials

The solvent used was 0.1 M NH_4NO_3, with 0.02% of sodium azide added. The flow rate was generally set to 0.8 mL/min (0.013 cm^3-s^{-1}), as was suggested for the Shodex columns, although some measurements were made at flow rates of 0.4 and 1.2 mL/min to explore the shear dependence of the viscosity measured. The pH of the solvent was unadjusted, and was about 6. Several polymers were used to assess the performance of the viscometers, one of which was bacterial sodium hyaluronate (HA) (Sigma Chemical Company, St. Louis, MO) with a nominal weight-average molecular weight of about $1.2 \cdot 10^6$ g-mol^{-1}, which was injected at a concentration of 0.2 mg/mL. The volume of sample injected in all cases was 250 μL. Sonication for a few hours of a portion of this material produced lower weight-average molecular weight samples, which were also used to characterize the viscometers.

Low polydispersity poly(oxyethylene) (POE), a gift from Dr. Jeanne François (ICS, Strasbourg, France), had a nominal weight-average molecular weight of 10^4 g-mol^{-1}, and was injected at a concentration of 4 mg/mL. Also measured were two dextran viscosity standards (gifts from Dr. Marshall Fishman, USDA, Philadelphia, Pa.) designated T110 and T500. T110 had a nominal weight-average molecular weight of 106 kg-mol^{-1} and a nominal intrinsic viscosity of 32.0 cm^3/g. T500 has a nominal weight-average molecular weight of 532 kg-mol^{-1} and a nominal intrinsic viscosity of 53 cm^3/g. Both were injected at a concentration of 3 mg/mL. Finally, a sample of poly(vinyl pyrolidone) (PVP) was injected at a concentration of

2 mg/mL. While this polymer had a nominal molecular weight of 1300 kg-mol^{-1}, our Zimm plot results showed a molecular weight of 870 kg-mol^{-1}. Table I describes these polymers.

ANALYSIS

In this paper we focus on the viscometers and their performance. Details of the use and analysis of the other detectors in this context exist in the literature.[21–26] Briefly, the RI detector gives the concentration of polymer at each elution point, given the increment of refractive index dn/dc. With this information, and given the second virial coefficient A_2, the MALLS detector provides the mass and radius of gyration of the eluting polymer at every sampled elution point. This is done using the Zimm equation,[27] which for $q^2 \langle R_g^2 \rangle_Z < 1$ is given by

$$\frac{Kc}{R_\theta} = \frac{1}{M_W}\left(1 + \frac{1}{3}q^2\left\langle R_g^2\right\rangle_Z\right) + 2A_2c \tag{4}$$

where q is the scattering wave vector given by $q = (\pi n/\lambda)\sin(\theta/2)$. That is, by measuring the scattered laser light (which gives the Rayleigh ratio R_θ) as a function of the scattering angle θ, one obtains the weight-average molecular weight M_W, and the Z-average mean square radius of gyration, $\langle R_g^2 \rangle_Z$, by using the measured value of the concentration c, and the known values of solvent refractive index n, laser wavelength λ, second virial coefficient A_2, and the constant K, which, for vertically polarized light is given by $(\pi n^2\ (\mathrm{dn/dc})^2)/(N_A\lambda^4)$, where N_A is Avogadro's number. The

TABLE I Polymers Used to Characterize the Viscometers

Polymer	*Injected concentration [mg-mL^{-1}]*	*Specific refractive index dn/dc [cm^3–g^{-1}]*	*Molecular weight [kg-mol^{-1}]*	*A_2 [cm^3-mol-g^{-2}]*
poly(oxyethylene)	4	0.141	10	0.0062
dextran-T110	3	0.142	106	*0.00045
dextran-T500	3	0.142	532	*0.000175
poly(vinyl pyrolidone)	2	0.173	1300	*0.00028
hyaluronic acid (sonicated)	1	0.155	*329	0.003
hyaluronic acid	0.2	0.155	*1300	0.003

No nominal values were available for entries marked*, as such, these entries are values measured for these experiments.

Rayleigh ratio for toluene of 0.00001408 cm^{-1} at 25°C and λ = 633 nm was used to convert relative scattered intensities of the samples into their Rayleigh ratios.

Single-Capillary Viscometer

Each of the viscometers depends for its function upon the prediction by Poiseuille's equation that a change in viscosity will result in a change in pressure drop provided that the volume flow rate remains constant. Thus, in the case of the single-capillary viscometer, the specific viscosity at each sampled elution point i, takes the simple form given by

$$\eta_{sp,i} \equiv \frac{\eta_i - \eta_0}{\eta_0} = \frac{P_i - P_0}{P_0} = \frac{V_i - V_0}{V_0} \tag{5}$$

where P_i represents the pressure drop along the capillary and V_i represents the voltage signal corresponding to that drop, both at elution point i. Note that the specific viscosity is unitless. P_0 and V_0 refer to the average solvent baseline values. Note that since the same transducer is used to measure all quantities in the expression, any calibration factors cancel in the ratio. Thus, no calibration is necessary. This is in contrast to the bridge viscometer, in which two transducers are used, both of which must be calibrated. Given the specific viscosity $\eta_{SP,i}$, the reduced viscosity at elution point i, $\eta_{R,i}$, follows directly from

$$\eta_{R,i} = \frac{\eta_{sp,i}}{c_i} \tag{6}$$

where c_i is the concentration at elution point i, obtained from the refractometer. The units of $\eta_{R,i}$ are inverse mass concentration, generally given as cm^3-g^{-1}. Note that hidden in the denominator, c_i, are the refractive index increment dn/dc, and the refractometer calibration factor CF. Any error in these two parameters causes a corresponding error in the reduced viscosity, and in the weight-average reduced viscosity (discussed later).

In error analysis, we assume that all random errors add in quadrature, and so, for a calculated quantity, $f = (u,v,w, \ldots)$, which is a function of several measured variables, $\{u,v,w, \ldots\}$, the error in f is calculated as

$$\sigma_f^2 = \left(\frac{\partial f}{\partial u}\right)^2 \sigma_u^2 + \left(\frac{\partial f}{\partial v}\right)^2 \sigma_v^2 + \left\langle \frac{\partial f}{\partial u}\frac{\partial f}{\partial v}\Delta u \Delta v \right\rangle + \ldots \tag{7}$$

where the brackets indicate an average over many measurements, with uncertainties Δu, Δv, etc. We assume that the parameters u and v are unrelated, and thus, over many measurements, the average of the errors will vanish (*i.e.*, the covariance of u and v is zero). The error (standard deviations) in the measured quantities (σ_u, σ_v, etc.) are calculated in the usual way as

$$\sigma_u^2 = \frac{1}{N-1}\sum_{i=1}^{N}(u_i - u_{AVG})^2 \tag{8}$$

where u_i is the i^{th} measured quantity in the baseline region and u_{AVG} is the average of u over the baseline region. Using the form of Equation (7) to calculate the fractional error in the reduced viscosity for the single-capillary viscometer, we obtain

$$\left(\frac{\sigma_{\eta_{R,i,SC}}}{\eta_{R,i,SC}}\right)^2 = \left(\frac{V_i^2 + V_0^2}{(V_i - V_0)^2}\right)\left(\frac{\sigma_V}{V_0}\right)^2 + \left(\frac{\sigma_C}{c_i}\right)^2 \tag{9}$$

where σ_V is the standard deviation of the voltage measured in the baseline region, and σ_c is the standard deviation of the concentration obtained from the RI detector in the baseline region. We see that the error divides into two types: errors in the measurement of the voltages from the transducer and error in the measurement of the concentration. With typical values of $\sigma_c \sim 10^{-7}$ g-cm^{-3} and $c_i \sim 10^{-5} - 10^{-4}$ g-cm^{-3} near the peak, the concentration error is on the order of 0.1–1%. Clearly these will be larger in the wings of a given mass distribution, and will conversely be smaller if a larger concentration is injected. The largest source of error is in the measurement of the pressure change as the polymer solution passes the detector. This is clearly seen if we recognize that generally, $V_i \approx V_0$ (the difference is generally a few percent). Then, the first term on the right side of Equation (9) is approximately $2[\sigma_V/(V_i - V_0)]^2$. We see that the relevant comparison is the amplitude of the voltage noise ($\sigma_V \sim 0.7$ mV) as compared to the difference between the solvent background and the polymer signal, as might be expected. This latter quantity will vary with experimental conditions (type of polymer, concentration of polymer, etc.), and even within a given measurement (larger in the wings of a polymer distribution than near the peak), but varies from about 11 mV for 10k mass POE injected at a concentration of 1 mg/mL to about 120 mV for 1200k mass HA injected at a concentration of 0.2 mg/mL, giving contributions due to voltage error of about 6 and 0.6%, respectively.

The weight-average reduced viscosity is defined as

$$\eta_{R,w} = \frac{\sum_{i=1}^{N} \eta_{R,i} c_i}{\sum_{i=1}^{N} c_i} = \frac{\sum_{i=1}^{N} (V_{SC,1} - V_0)}{V_0 \sum_{i=1}^{n} c_i} \tag{10}$$

where the sum is over the peak of the eluted polymer distribution. Again, we see that systematic calibration errors affecting the refractometer cause corresponding errors in the viscosity. Considering only random measurement error, and following Equation (7) in the error calculation, we obtain

$$\left(\frac{\sigma_{\eta_{R,w}}}{\eta_{R,w}}\right)^2 = N\left(\frac{\sigma_V}{\sum_{i=1}^{N}(V_i - V_0)}\right)^2 + \frac{\sum_{i=1}^{N} V_i^2}{\left(\sum_{i=1}^{N}(V_i - V_0)\right)^2}\left(\frac{\sigma_V}{V_0}\right)^2 + N\left(\frac{\sigma_c}{\sum_{i=1}^{N} c_i}\right)^2 \tag{11}$$

for the fractional error in the calculation of the weight-average viscosity, where N is the number of points used in the average. The first term originates from error in measuring V_i, the second term from error in measuring the background V_0, and the third from random errors in measuring the concentration. In computing the error due to V_0, it (V_0) is not factored out of the denominator of Equation (10), rather differentiated with respect to in each of the N terms, since uncertainty in η_R due to V_0 is present in each term. We can estimate the relative magnitudes of the first two terms by recognizing that $V_i \approx V_0$ and so the second term is roughly the same as the first (in fact, exact calculation shows them to be almost identical). If we write $\Sigma(V_i - V_0) \approx N \cdot \delta V$, where δV is the average voltage difference, then the first two terms contribute $(2/N)^{1/2}$ ($\sigma_v/\delta V$) to the error. The number of terms in a sum is typically between 50 and 100, and with $\sigma_v \sim 0.7$ mV and $\delta V \sim 10$–100 mV, we can estimate the contribution from errors in voltage as roughly 0.1–1.4%. In practice, the voltage error in Equation (11) varies from about 2% for 10k mass POE injected at 1 mg/mL, to 0.13% for 1200k mass HA injected at 0.2 mg/mL. Doing likewise with the error due to concentration measurement, we obtain a contribution of $N^{-1/2}$ ($\sigma_c/\delta c$) ~ 0.01–0.1%, using $\sigma_c \sim 10^{-7}$ g-cm^{-3} and $\delta c \sim 10^{-5}$–10^{-4}g-cm^{-3}. We see that the error due to measurement of the pressure change generally dominates that due to

measuring the concentration, and so combined error is of the order of 0.1–1.4%. Note that all three terms benefit from averaging in that their contribution in Equation (11) varies as N^{-1} (notice that there are N terms in the sums in the denominator), which follows from the assumption that the errors add in quadrature.

Bridge Viscometer

A sketch of the bridge viscometer is shown in Figure 1. In this case, the specific viscosity takes the form

$$\eta_{sp,i} \equiv \frac{\eta_i - \eta_0}{\eta_0} = \frac{4P_{\Delta,i}}{P_{B,i} - 2P_{\Delta,i}} = \frac{4K_\Delta V_{\Delta,i}}{K_B V_{B,i} - 2K_\Delta V_{\Delta,i}} \tag{12}$$

where P_Δ is the pressure difference between the two arms of the bridge, P_B is the pressure drop across the arms of the bridge, and K_Δ and K_B are the calibration constants needed to convert the voltage received from the two transducers into the respective pressure drops. Note that since two different

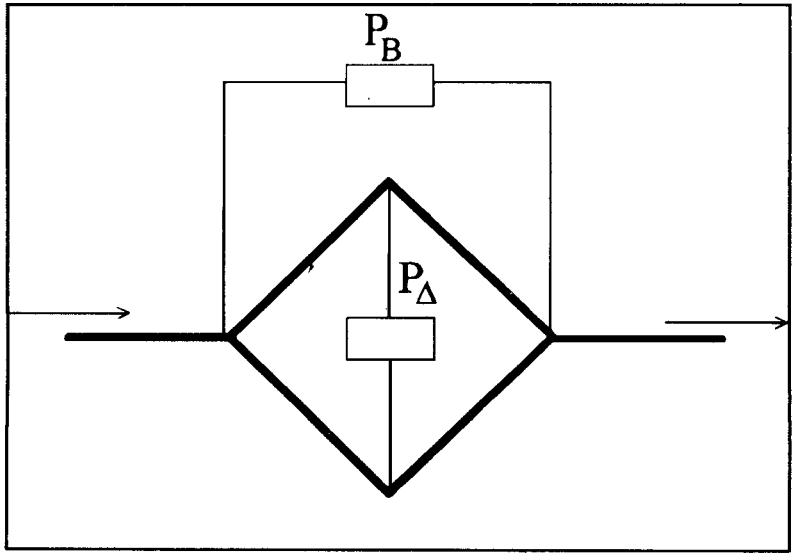

FIGURE 1 Diagram of the bridge viscometer design, showing the background (P_B) and differential (P_Δ) pressure transducers. Not shown is the takeup reservoir in one arm of the bridge, which delays elution of approximately half of the injected sample for approximately 30 mL.

transducers are used, the calibration constants do not cancel as is the case for the single-capillary viscometer. This represents a potential source of systematic error in viscosity determinations using the bridge viscometer. So long as $P_\Delta \ll P_B$ (the former is at most a few percent of the latter), the fractional error in $\eta_{sp,i}$ due to errors in the calibration constant is equal to the fractional error in the constant determination, and can thus be ignored if these errors are small. However, we find that errors in measuring η_{sp} from other sources are routinely a few percent or less, and thus the calibration constants must be known to at least this accuracy. In our case, we calibrated the two detectors by measuring the pressure drop along a capillary (whose length and inner diameter was known) as the volume flow rate was increased from 0 to 1 mL/min. The slope of a line fit to the voltage thus obtained, plotted as a function of the pressure drop (obtained from Poiseuille's equation) provides the needed calibration constant. The standard deviation in K_B, the calibration constant for the bridge (P_B) transducer, was about 0.3% and that of K_Δ, for the differential (P_Δ) transducer, was about 1.3%, suggesting that the calibration constants are known to that accuracy. The former is less than, or of the order of the other errors in the bridge viscometer measurements, whereas the latter is of the same order of larger and is presumably a significant source of systematic error in these measurements.

Considering only random errors during measurement, as opposed to systematic error due to inaccuracies in calibration, the fractional error in the specific viscosity, again following Equation (7), is given by

$$\left(\frac{\sigma_{sp,i}}{\eta_{sp,i}}\right)^2 = \left(\frac{K_B V_{B,i}}{K_B V_{B,i} - 2K_\Delta V_{\Delta,i}}\right)^2 \left[\left(\frac{\sigma_{V_\Delta}}{V_{\Delta,i}}\right)^2 + \left(\frac{\sigma_{V_B}}{V_{B,i}}\right)^2\right] \tag{13}$$

where $\eta_{sp,i}$ is given by Equation (12) and $\sigma_{V\Delta}$ and σ_{VBB} are, respectively, the standard deviation of the differential and bridge transducer measurements, evaluated in the baseline region. Since P_B ($=K_B V_B$) is much greater then P_Δ ($= K_\Delta V_\Delta$), we can write the fractional error in $\eta_{sp,i}$ in the intuitive form

$$\left(\frac{\sigma_{\eta sp,i}}{\eta_{sp,i}}\right)^2 \approx \left(\frac{\sigma_{V_\Delta}}{V_{\Delta,i}}\right)^2 + \left(\frac{\sigma_{V_B}}{V_{B,i}}\right) \tag{14}$$

although in our calculations we use the form of Equation (13). Equation (14) shows that the fractional error in $\eta_{sp,i}$ is due in equal measure to errors in measuring $V_{\Delta,i}$ and $V_{B,i}$. Typically, the standard deviation in both $V_{\Delta,i}$ and

$V_{B,i}$ was about 0.2 mV. With $V_{B,i} \approx 0.2$ V, the fractional error due to background measurement (the second term of Equation (14)) is about 0.1%. The differential transducer voltage, $V_{\Delta,i}$, varies with experimental conditions, but varies from about 60 mV for 10k mass POE injected at 1 mg/mL, to about 500 mV for 1200k mass HA injected at a concentration of 0.2 mg/mL. This gives an error due to differential voltage measurement of about 0.04–0.3%. Thus, the two sources of error shown in Equation (14) are roughly comparable.

The reduced viscosity at elution point i is again given by Equation (6). The fractional error in the reduced viscosity can be written as

$$\frac{\sigma^2_{\eta_{R,i}}}{\eta^2_{R,i}} = \left[\left(\frac{\sigma_{\eta_{sp,i}}}{\eta_{sp,i}}\right)^2 + \left(\frac{\sigma_c}{c_i}\right)^2\right]^2 \tag{15}$$

where $\sigma_{\eta sp,i}$ is given by Equation (13) and σ_c is the standard deviation in the concentration measurement. Recalling that the fractional error in concentration is of order 0.1–1%, we see that for the bridge viscometer, the fractional error in the reduced viscosity is, in general, dominated by the error in the concentration measurement. With the use of the typical values mentioned, the fractional error in reduced viscosity from all sources varies from about 0.1–1%, to be compared with 0.6–6% in the case of the single-capillary design. This shows the greater precision evidenced by the bridge viscometer design. Again, the weight-average reduced viscosity is given by

$$\eta_{R,w} = \frac{\sum_{i=1}^{N} \eta_{R,i} c_i}{\sum_{i=1}^{N} c_i} = \frac{\sum_{i=1}^{N} \eta_{sp,i}}{\sum_{i=1}^{N} c_i} \tag{16}$$

where the sum is again taken over the peak of the polymer distribution. The fractional error is then given by

$$\left(\frac{\sigma_{\eta_{R,w}}}{\eta_{R,w}}\right)^2 = \frac{\sum_{i=1}^{N} \sigma^2_{\eta sp,i}}{\left(\sum_{i=1}^{N} \eta_{sp,i}\right)^2} + N\left(\frac{\sigma_c}{\sum_{i=1}^{N} c_i}\right)^2 \tag{17}$$

Note that the error again divides naturally into a term due to errors in measuring the voltages from the viscometer, and a term due to errors in measuring the concentration. By substitution of the variables in each

summation with a mean value, and with N ~ 100, the error in viscometer measurement is given by $N^{-1/2} \cdot \langle \sigma_{\eta sp,1} \rangle / \langle \eta_{sp,i} \rangle \sim 0.01–0.1\%$. Recall that the concentration error is of the order of 0.01–0.1%, of the same order as the viscometer error, giving a fractional error in weight-averaged reduced viscosity of 0.01–0.1%. Comparing this with the single-capillary viscometer result of 0.1–1.4%, we again see the increased precision of the bridge design. Note that, as in the case of the single-capillary design, each error term varies as N^{-1} (each denominator varies as N^2), and thus both obtain a benefit from averaging.

We use the equations developed in this section to calculate viscosities and errors in the following section, in which the experimental results are presented.

RESULTS

In Figure 2, we show a typical baseline region for the two viscometers. The upper two curves show the behavior when using the ISCO 2350 HPLC pump and the lower two curves show the results with the Hewlett Packard Series 1100 isocratic pump. In each pair (upper and lower), the upper curve of the pair shows the Viscotek Model 100 differential viscometer measurement (which has been deliberately shifted to facilitate the comparison), and the lower of the pair shows the single-capillary measurement. The most striking difference is between the two different pumps, and the effect of pump pulsing on the viscometer measurements. Each pump has an intrinsic pulse damper, which was optimized by adjusting for the compressibility of the solvent. In a further attempt to minimize pump pulsing, a separate pulse damper was added external to the pumps, with minimal effect. In both cases, the noise from the ISCO pump pulsation is several times that of the HP pump; proper choice of the HPLC pump is crucial to optimize on-line viscometer measurements.

A second observation is that, for a given pump, the noise in the single-capillary viscometer signal is a few times that of the bridge viscometer, showing one of the significant benefits of the bridge design. Note again, however, that the proper choice of pump is crucial to realize the potential benefits of the bridge viscometer. In fact, one observes in Figure 2 that using the bridge viscometer with a pump which generates significant pulsing gives worse performance than the single-capillary viscometer when used with a pump which shows minimal pulsing.

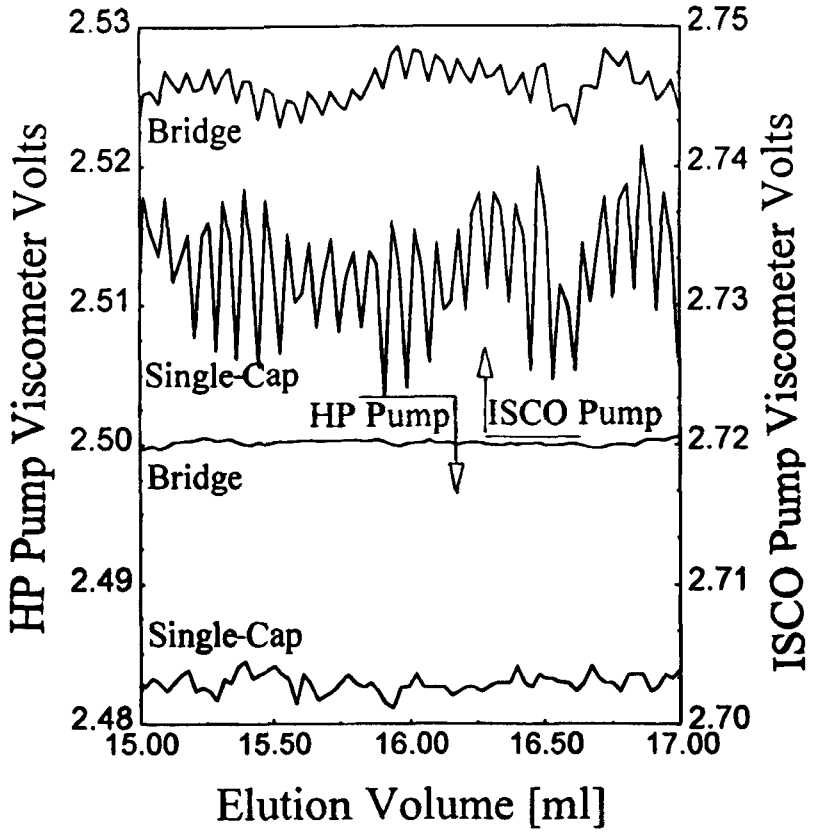

FIGURE 2 Solvent signal from both viscometers, using both pumps. Top two curves show data obtained using the ISCO pump, while lower two curves show data obtained using the Hewlett Packard pump. The top curve of each pair is the differential signal from the bridge viscometer (which has been deliberately offset to facilitate the comparison), while the lower of each pair is that from the single-capillary viscometer. The considerable benefit of a pump which minimizes pulsation is evident. Note also that the bridge viscometer gives superior performance with a given pump, but the single capillary viscometer, when coupled with a superior pump, gives cleaner data than the bridge viscometer with a noisy pump.

In addition to the noise resulting from cyclical pressure variations induced by the pump pistons, we also observed sudden and random pressure drops, followed by a recovery to normal baseline, caused by the use of improperly degassed mobile phase. As with the more transient signals just discussed, the distortion in the viscometer signals was present in both viscometers, but was stronger in the single-capillary design. Recall that the

design of the bridge viscometer makes it less susceptible to deviations in flow rate, since it depends on ratios of flow rates through the arms of the viscometer, rather than on the absolute flow rate as in the single-capillary design. Reliable results from both viscometers, but particularly the single-capillary design, demand a reliable and stable flow rate.

To further indicate the difference between the two pumps, we show in Figure 3 two single-capillary viscometer tracings for POE (molecular weight 10 kg/mol) injected at a concentration of 4 mg/mL. The reduced noise in the case of the HP pump is clear. (One may also observe that the earlier, ISCO peak is narrower and higher in magnitude. This is due to degradation of the columns in the course of the experiments, which lasted over a year: 9800 equivalent plates were calculated in the earlier ISCO measurements, and about 4300 equivalent plates in the later HP measurements. We stress that this was not connected with the change in pumps.)

In Figure 4a–c, we show the signals from all four detectors when injecting POE, at a concentration of 4 mg/mL. From top to bottom, Figure 4a shows the refractive index signal (which provides an independent measurement of the concentration), Figure 4b the light scattering signal at 90 degrees (which, with the data from the other angles and the concentration, gives the mass and radius of gyration), and Figure 4c the two viscometer signals, superimposed in one graph. As is evident, the data are very clean, and no smoothing was ever necessary, even for such weak signals as are shown here. Also, one can see that the two viscometer tracings are completely consistent with one another as the superposition of the two tracings shows, although the bridge viscometer clearly returns a cleaner signal. Finally, the volume separations between the three detectors are evident here and were determined by measuring the separation between the peaks (the mass distribution of this material was narrow enough, $M_W/M_n \sim 1.03$, that one expects the peaks to superpose when volume separation between detectors is accounted for). This was checked by making several injections through the system, but without the columns to minimize spreading of the elution peak. Peak locations were determined by fitting parabolas to the top of the peaks and using the position of the parabola maximum. The results were consistent, and the volume separation between detectors was 0.20 mL between MALLS and refractometer, 0.56 mL between refractometer and single-capillary viscometer, and 0.20 mL between the single-capillary and bridge viscometers. Note that this is a low-mass polymer at a reasonably small concentration, and thus represents a significant test of the systems capabilities.

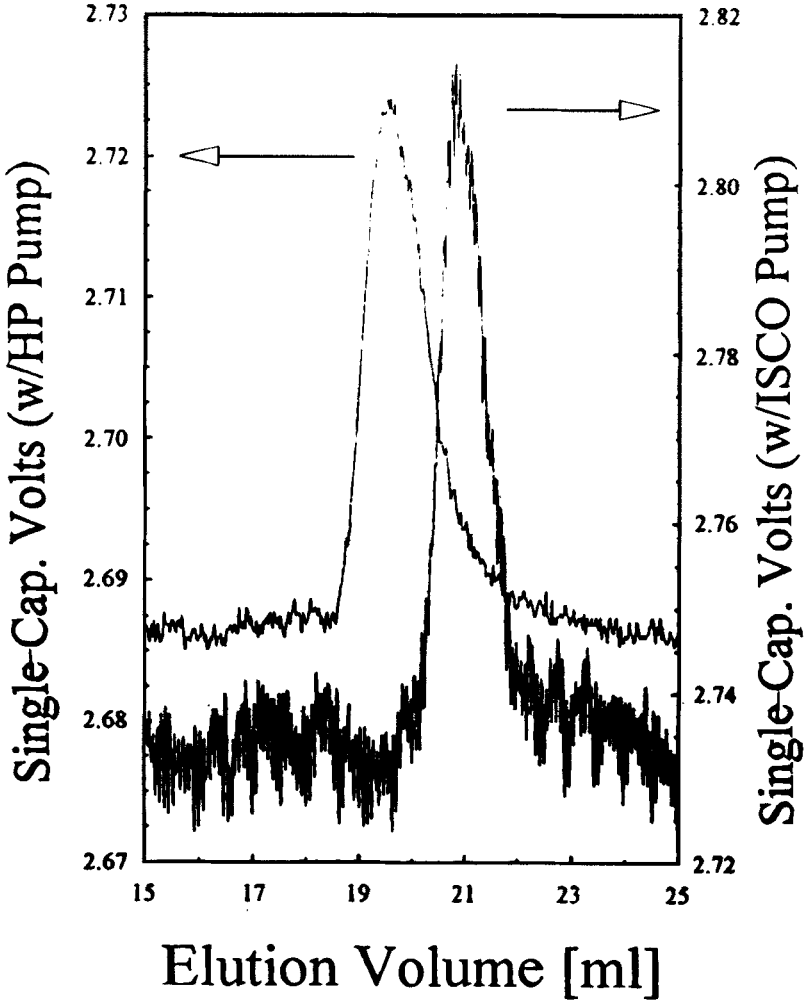

FIGURE 3 Signal obtained from the single-capillary viscometer when injecting poly(oxyethylene), and using the ISCO pump (right axis) and the Hewlett Packard pump (left axis). Difference in signal to noise is clear.

Figure 5a–c shows similar data for a large mass polymer, ultrasonically degraded hyaluronic acid (HA) with a weight-average molecular weight of 329 kg-mol^{-1}, injected at a lower concentration, 1.0 mg/mL. Again, the raw signals are very clean and for this high molecular weight sample, the two

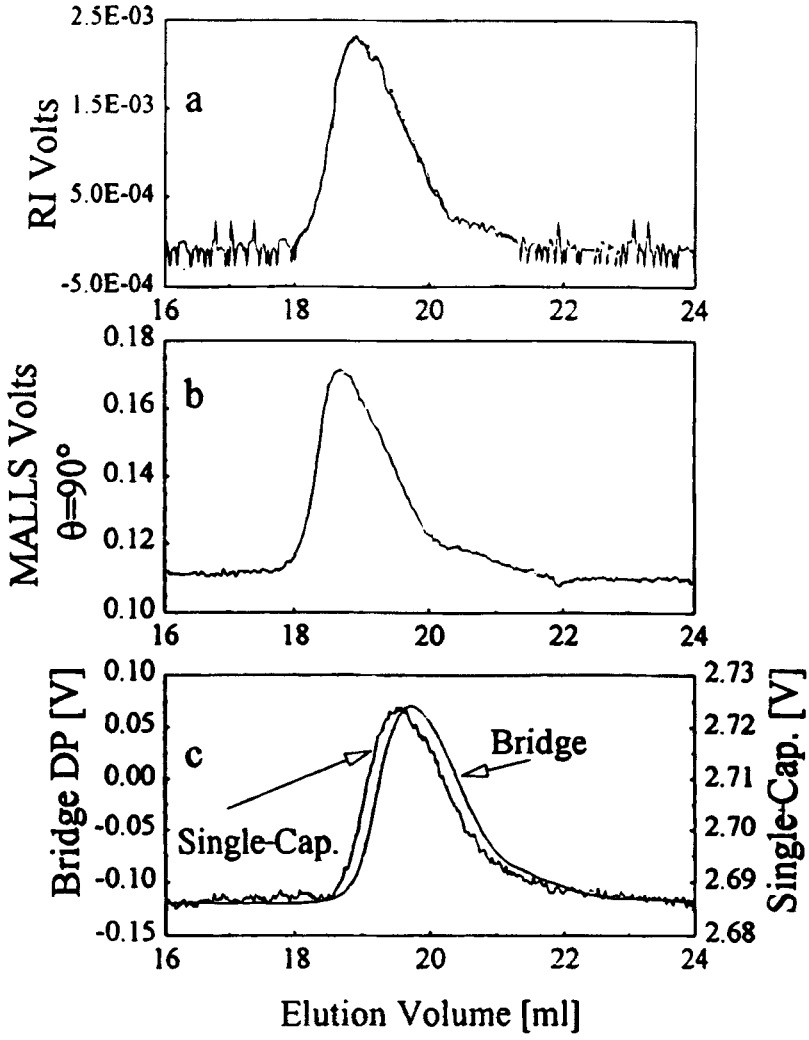

FIGURE 4 Raw voltage signals from the four detectors, as a function of elution volume, when injecting poly(oxyethylene): a) refractometer, b) MALLS detector at $\theta = 90°$, c) single-capillary viscometer (right axis) and differential signal from the bridge viscometer (left axis).

viscometer signals are identical in shape and virtually identical in signal to noise, showing that for larger viscosities (*i.e.*, larger molecules and/or larger concentrations) the relative advantage of the bridge viscometer is significantly reduced.

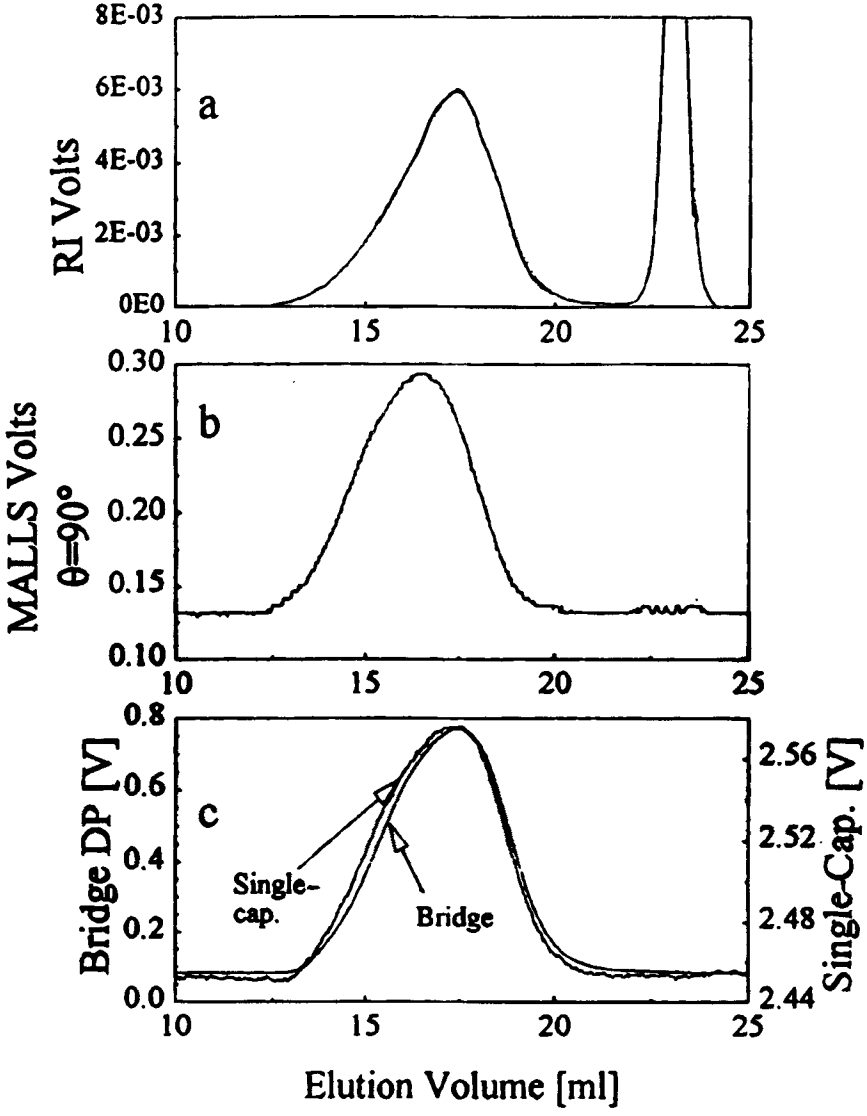

FIGURE 5 Raw voltage signals from the four detectors, as a function of elution volume, when injecting hyaluronan: a) refractometer, b) MALLS detector at $\theta = 90°$, c) single-capillary viscometer (right axis) and differential signal from the bridge viscometer (left axis).

In Figure 6a–b, we show the calculated results obtained from the data in the previous figure. In Figure 6a, we plot the concentration, in g-cm^{-3}, and the radius of gyration, in cm, both as a function of the mass. Note that the mass and R_g axes are logarithmic. Below, in Figure 6b, we show a log-log plot of the reduced viscosity obtained from both the single-capillary (upper curve) and bridge (lower curve) viscometers. We assume that the concentrations are low enough that the reduced viscosity is sufficiently close to the intrinsic viscosity. The agreement between the viscosities obtained from the two viscometers is excellent, although there is a slight systematic decrease in the viscosity from the bridge viscometer, discussed below.

In Table II, we summarize the experimental results. Note that two of the entries show the polydispersity as measured by the ratio of the Z-average squared radius of gyration, $\langle R_g^2 \rangle_Z$, to the weight-average squared radius of gyration, $\langle R_g^2 \rangle_W$, and the ratio of the weight-average squared radius of gyration, $\langle R_g^2 \rangle_W$, to the number-average squared radius of gyration, $\langle R_g^2 \rangle_n$. Whenever the radius of gyration scales as a power of the molecular weight (*i.e.*, $R_g \sim M^\alpha$), then these ratios are given by

$$\frac{\langle R_g^2 \rangle_Z}{\langle R_g^2 \rangle_W} = \frac{1}{M_w} \frac{\int M^{2\alpha} M c(M) dM}{\int M^{2\alpha} c(M) dM} \tag{18}$$

and

$$\frac{\langle R_g^2 \rangle_W}{\langle R_g^2 \rangle_n} = \frac{1}{M_n} \frac{\int M^{2\alpha} c(M) dM}{\int M^{2\alpha} (c(M)/M) dM} \tag{19}$$

For an ideal random coil, $\alpha = 0.5$, and the ratios above simplify to

$$\frac{\langle R_g^2 \rangle_Z}{\langle R_g^2 \rangle_W} = \frac{M_Z}{M_W} \tag{20}$$

and

$$\frac{\langle R_g^2 \rangle_W}{\langle R_g^2 \rangle_n} = \frac{M_W}{M_n} \tag{21}$$

That is, for an ideal random coil, the polydispersity as measured by the ratio of the mass averages is the same as the polydispersity as measured by the ratio of the radius of gyration averages. For $\alpha > 0.5$, the ratio of R_g^2 averages shown above are greater than the corresponding ratios of mass averages, and

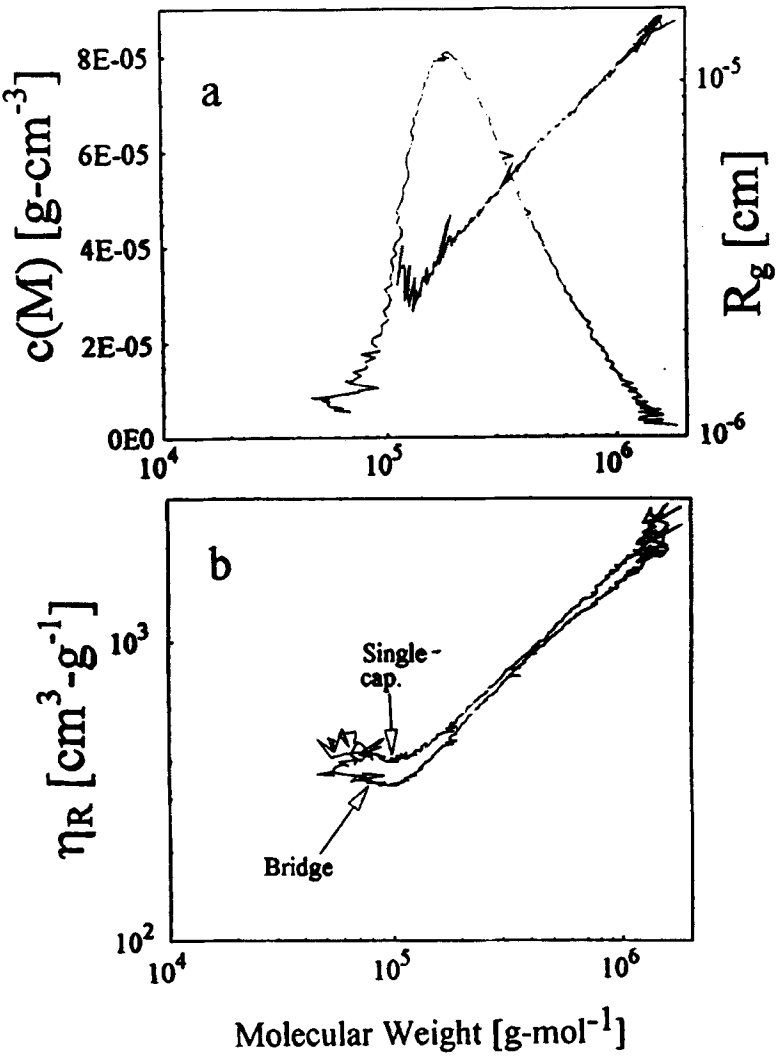

FIGURE 6 Polymer properties calculated for HA from the data in Figure 5. a) Concentration, $c(M)$ (from Equation (1)), and radius of gyration, $R_g(M)$, at each elution point, as a function of molecular weight, M (R_g and M from Equation (4)). b) Reduced viscosity, $\eta_R(M)$ ($\equiv[\eta](M)$), at each elution point, from the bridge (Equation (15)) and single-capillary viscometers (Equation (6)), plotted as a function of molecular weight, M. Note in b) that the viscosity as measured by the bridge viscometer is slightly lower than that measured by the single-capillary viscometer. Note also that, except for the ends, where concentration and thus signal to noise are low, the viscosity and radius of gyration show the expected power law dependence on M.

TABLE II Summary of Experimental Results from SEC Measurements on Several Polymers

Properties	*POE*	*PVP*	*T500*	*T110*	*HA*	*HA*
molecular weight, M_W [kg-mol^{-1}]	10.1 ± 0.22	801 ± 47	562.5 ± 3.5	103.6 ± 2.8	328.9 ± 7.8	1300 ± 210
polydispersity M_Z/M_W	1.05 ± 0.04	1.64 ± 0.02	2.23 ± 0.09	1.05 ± 0.008	1.60 ± 0.05	1.13 ± 0.09†
polydispersity M_W/M_n	1.03 ± 0.02	1.79 ± 0.02	1.73 ± 0.01	1.06 ± 0.02	1.44 ± 0.02	1.15 ± 0.09†
$R_{g,Z}$ [Å]	na	475 ± 18	179 ± 13	na	7 51 ± 30	1400 ± 240
$R_{g,W}$ [Å]	na	381 ± 23	111 ± 18	na	557 ± 26	1300 ± 170
$R_{g,n}$ [Å]	na	301 ± 37	72 ± 18	na	430 ± 13	1190 ± 120
$\langle R_g^2\rangle_Z/\langle R_g^2\rangle_W$	na	1.56 ± 0.08	2.56 ± 0.37	na	1.81 ± 0.08	1.16 ± 0.13†
$\langle R_g^2\rangle_W/\langle {}^2{}_g\rangle_n$	na	1.63 ± 0.03	2.57 ± 0.56	na	1.66 ± 0.04	1.19 ± 0.13†
$[\eta]_W$ [cm^3-g^{-1}] Single-Capillary*	25.3 ± 2.5	125 ± 134	41.7 ± 5.1	22.0 ± 2.6	772 ± 28	2460 ± 95

(continued)

TABLE II (*Continued*)

Properties	*POE*	*PVP*	*T500*	*T110*	*HA*	*HA*
$[\eta]_W$ [cm^3-g^{-1}] Bridge*	23.5 ± 1.3	132 ± 4	39.3 ± 0.6	24.0 ± 1.4	718 ± 23	1790 ± 30
$k'_{R,}$	na	0.73 ± 0.19	smallM–	na	0.20 ± 0.11	na
R_g prefactor			2.06 ± 0.56 largeM– 0.576 ± 0.20			
α' R_g exponent	na	0.45 ± 0.015	smallM- 0.56 ± 0.023 largeM- 0.31 ± 0.020	na	0.63 ± 0.039	na
$k'_{[\eta]}$, [η] prefactor	na	0.18 ± 0.04	smallM– 1.23 ± 0.25 largeM– 9.04 ± 0.41	na	0.10 ± 0.02	na
a' [η] exponent	na	0.46 ± 0.014	smallM- 0.27 ± 0.015 largeMC 0.12 ± 0.003	na	0.70 ± 0.010	na

*Reduced viscosities $\eta_{R,W}$, normally expected to be quite close to the intrinsic viscosity.
†These low polydispersities may indicate that the unsonicated HA elutes in the exclusion volume of the columns.
The errors shown are the standard deviation of several measurements, which is considerably larger than the calculated random error in any one measurement.

vice versa for $\alpha < 0.5$. From the table, we see that the ratios of the R_g^2 averages are generally a little larger than the ratios of the mass averages. Note also that the errors for the former are larger than the errors of the latter. This is to be expected since the error in R_g is generally larger than that of the mass.

The R_g and $[\eta]$ coefficients and exponents given in Table II were obtained by fitting equations of the form

$$R_g = k_R' M^{\alpha'} \tag{22}$$

and

$$[\eta] = k_{[\eta]}' M^{\alpha'} \tag{23}$$

Note that these are only available when the injected samples are polydisperse, since it is only in that case that a reasonable range of masses is obtained in the measurement. Since T500 has different exponents (and thus different coefficients) in different mass ranges, it has two entries for those quantities. The results shown are averages from many different experiments performed on several different days, each of which had its own error calculated according to the expressions developed in the analysis section. The error shown is either the quadrature sum of the random errors in each measurement, or the standard deviation of averaged values over many measurements, whichever is larger. In virtually every case, however, the dominant error stems from the variation in results from one run to the next rather than from the random error in any one experiment. For example, the weight-average viscometry data for sonicated hyaluronic acid generally produce a precision of roughly 0.1% for the single-capillary viscometer and a small fraction of this for the bridge viscometer. Cumulative results, however, gave an error, as indicated, of a little over 3% in each case.

Table III summarizes the fractional errors in the weight-average viscosity obtained from the two viscometers due to random errors in a given measurement, systematic errors due to errors in instrument calibration, and error due to variations over many runs. We see that the dominant error in both viscometers is that due to run to run variations.

The molecular weights shown in Table II agree well with the nominal values, where available. Except for the hyaluronic acid, the weight-average viscosities obtained from the two viscometers agree well with each other, although the results for the two dextran samples are slightly lower than the nominal values. Possibilities here are calibration error in the refractometer,

TABLE III Summary of Sources of Error in the Weight-average Viscosity, and Typical Values for Each

Source of Error in $[\eta]_W$	*Bridge Viscometer*	*Single-Capillary Viscometer*
random measurement error		
A. background volts	~0.01–0.1 %	~0.1–1 %
B. differential volts	~0.01–0.1 %	~0.1–1 %
C. concentration	~0.01–0.1 %	~0.01–0.1 %
Instrument calibration		
A. viscometer	~1 %	none
B. refractometer	~1 %	~1 %
stochastic run-to-run error	1.5–6 %	3–12 %

Instrument calibration error is inferred from the standard deviation in the linear fits performed to calibrate the instruments. Run-to-run error is the standard deviation in the average values determined from many measurements.

or errors in dn/dc. The dn/dc used is the nominal literature value, and is the same as that used by the source of the nominal value of viscosity. Error in the calibration of the refractometer should cause deviations in both the molecular weight and the viscosity in the same direction (overestimation of one would imply overestimation of the other and vice versa). Since the molecular weights were slightly higher than the nominal values, we conclude the difference is not due to error in calibrating the refractometer.

In the case of the hyaluronic acid, the results from the single-capillary viscometer are in accord with published values by Fouissac *et al.*,[28] who used a Contraves low-shear viscometer to obtain extrapolations of reduced vicosity to zero concentration and zero shear rate to determine $[\eta]$ of HA in a solution of water with 0.1 M NaCl: they obtain $[\eta] = 2300$ cm^3-g^{-1} for $M_W = 1.35 \cdot 10^3$ kg-mol^{-1} (compare our result of $[\eta] \equiv \eta_{R,W} = 2460$ cm^3-g^{-1} for $M_W = 1.3 \cdot 10^3$ kg-mol^{-1}) and $[\eta] = 750$ cm^3-g^{-1} for $M_W = 3.5 \cdot 10^2$ kg-mol^{-1} (compare our result of $[\eta] \cong \eta_{R,W} = 770$ cm^3-g^{-1} for $M_W = 3.3 \cdot 10^2$ kg-mol^{-1}). Note, however, that the result from the bridge viscometer is significantly smaller than the that from the single-capillary. Since the inner diameter of the capillaries used is different for the two viscometers, there is a significant difference in average shear. For the single-capillary, the inner diameter is 0.020 in. and for the bridge viscometer, the inner diameter is 0.010 in. At a flow rate of 0.8 mL/min, this gives an average shear rate of 690 s^{-1} for the single-capillary viscometer and 5500 s^{-1} for the bridge viscometer. Thus, the difference in the two results could be due to shear thinning in the bridge viscometer. In Figure 7a–b, we show data taken for the

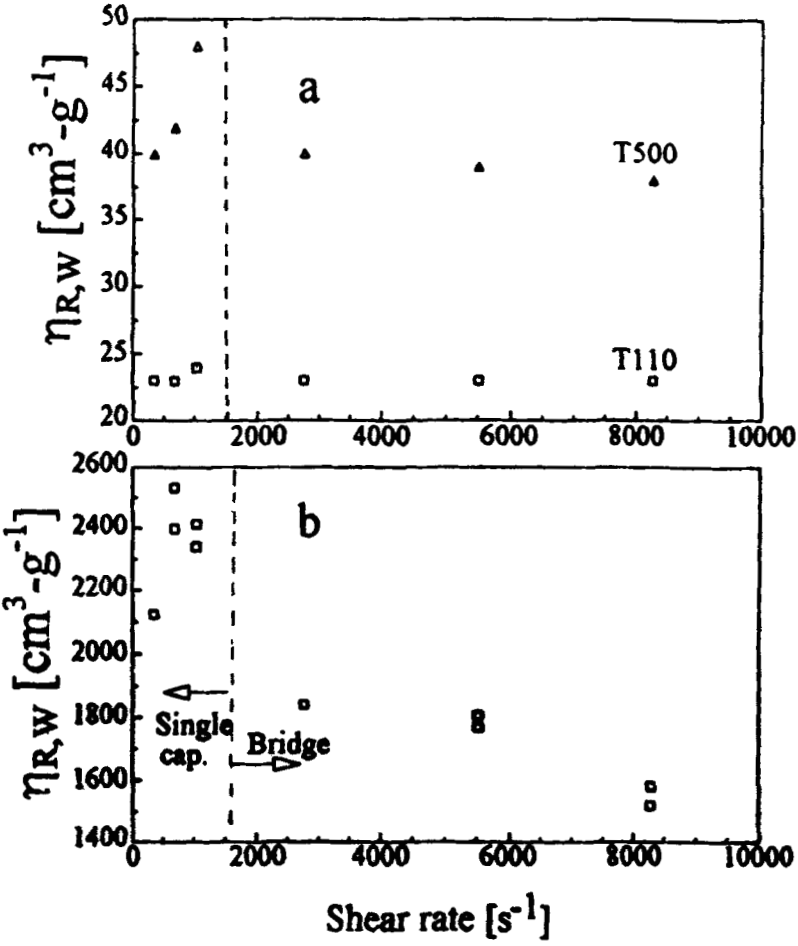

FIGURE 7 Weight-average reduced viscosity, $\eta_{R,W}$ ($\equiv[\eta]_W$), as a function of shear rate. Shear rates less than about 1100 s^{-1} correspond to measurements using the single-capillary viscometer, while those above 1100 s^{-1} correspond to the bridge viscometer. a) Results for dextran T500 (upper curve) and T110 (lower curve). Note no clear shear dependence. b) Results for hyaluronan. Note definite decrease in viscosity for increasing shear.

three different flow rates; 0.4, 0.8, and 1.2 mL/min, and with three different samples. Figure 7a shows the weight-average viscosity, as a function of shear rate, for the T110 and the T500. Figure 7b shows the same plot for the higher molecular weight hyaluronic acid ($M_W = 1.3 \cdot 10^3$ kg-mol^{-1}). No shear dependence is seen for the smaller dextran molecules, but shear

thinning is seen in the hyaluronic acid data above a shear rate of about 10^3 s^{-1}. This reinforces the conclusion that the difference between the HA data in Table II is due to shear thinning in the bridge viscometer.

Note that the results for the single-capillary viscometer are within the error bars indicated by the standard deviations in Table II, and thus the seeming increase in $\eta_{R,W}$ with increasing shear is most likely due to experimental uncertainty.

This evidence of shear-thinning reinforces the fact that, strictly speaking, what is measured in SEC viscometry is not the intrinsic viscosity, since extrapolation to zero shear and zero concentration is not performed. Since the viscosity will be a function of shear rate, and shear rate is a function of radius in the capillary, viscosity will implicitly depend on the capillary radius, and so one is not justified in using Poiseuille's equation to relate pressure drop to viscosity. For most of the polymers on which we report, and particularly at the concentrations used in these measurements, we expect these effects to be minor. That is, the concentrations are so small that the reduced viscosity is about equal to the intrinsic viscosity, and small enough that the shear dependence of viscosity is very weak (but note that this clearly fails for the bridge viscometer data on HA). Under these conditions, one can make a quasi-static approximation and assume that Poiseuille's equation holds, if the viscosity is replaced by some average viscosity. Integrating the flow equations, one finds that the appropriate average viscosity is

$$\eta_{AVG} = \langle \eta^{-1} \rangle^{-1} = \left[\frac{1}{\pi R^2} \int_0^R \frac{2\pi r dr}{\eta(r)} \right]^{-1}, \tag{24}$$

where R is the inner radius of the capillary, and r is any distance from the center of the capillary (but clearly less than R). One also finds that the condition on the variation of η with r is that $\eta^{-1}(r)$ must vary much more slowly than r. If these conditions are not fulfilled, then the variation of η with r must be modeled, and the flow equations solved to reliably relate the desired viscosity to the measured pressure drop.

It is generally held that the concentration of the injected solution c_{inj} should be below the overlap concentration of the polymer, often denoted as c*, in order to avoid separation artifacts in the columns. c* is often approximated as $[\eta]^{-1}$, since this latter quantity is mass per unit of hydrodynamic volume for a single polymer, and a solution concentration above this implies that indi-

vidual polymers interpenetrate each other. Comparison of injected concentrations in Table I with $[\eta]_W$ in Table II for each polymer show that $c_{inj} < [\eta]^{-1}$, although for the HA, the injected concentrations approach $[\eta]^{-1}$.

Since dextran is a branched molecule, it is not surprising that it has no unique power law,[3] but the values are not in agreement with what one expects. Specifically, a power higher than 0.5 for R_g versus M in a branched molecule is surprising. The poly(vinyl pyrolidone) is expected to behave as a random coil, giving a power law of 0.5 for both relations,[10] but the observed exponents are smaller. One would expect the same for HA, whose exponents are larger than the expected 0.5.[10] Even considerations such as self-avoiding walks and electrostatic excluded volume should give a power for R_g versus M of no more than about 0.60. Finally, if the radius of gyration scales linearly with the hydrodynamic radius, one expects that the two exponents would obey the relation $a' = 3\alpha' - 1$, which they do not.

Effect of Differential Fractionation

At each elution point i, MALLS measure the weight-average molecular weight and the Z-average radius of gyration, and the viscometers give the weight-average viscosity. If, as is generally presumed, the distribution measured at each elution point is monodisperse, these distinctions are meaningless. However, if the distribution measured is polydisperse, they are of concern. This polydispersity could be due, for example, to incomplete fractionation by the columns, or to diffusion remixing the polymer after fractionation. In general, the polydispersity due to these effects may vary from one elution point to another, an effect which may be termed "differential fractionation". The peak-broadening in Figure 3, suggesting as it does degradation of the column performance, leads us to consider the effect of polydispersity at each elution point on the scaling relations given by Equations (22) and (23).

Suppose that at each elution point, the sample measured is polydisperse obeying a log-normal distribution, with a peak value and width unique to each elution point. That is, assume that for the i^{th} elution point, the weight fraction of polymers with molecular weights between M and $M + dM$ is given by

$$W(M)dM = \frac{\exp\left\{-(\ln M - \ln M_i)^2 / 2\sigma_i^2\right\}}{\sqrt{2\pi}\,\sigma_i} dM \qquad (25)$$

The overall concentration profiles obtained from the refractometer/MALLS data roughly fit Equation (25), so that the form given has some experimental justification in this work. In any event, the qualitative conclusions presented do not depend on the particular form of the distribution. They do, however, require that the distribution be assymetric. The average molecular weight returned by the MALLS is weighted by this distribution, and is then given by

$$M_{W,i} = \frac{\int_{-\infty}^{+\infty} MW(M)dM}{\int_{-\infty}^{+\infty} W(M)dM} = M_i \exp[\sigma_i^2 / 2] \tag{26}$$

The Z-average R_g^2 is also returned by the MALLS, and is given by

$$\langle R_g^2 \rangle_{Z,i} = \frac{\int_{-\infty}^{+\infty} R_g^2 MW(M)dM}{\int_{-\infty}^{+\infty} MW(M)dM} = k_R^2 M_i^{2\alpha} \exp[2\alpha(\alpha+1)\sigma_i^2] \tag{27}$$

where we have assumed that R_g varies with mass as

$$R_g = k_R M^{\alpha} \tag{28}$$

That is, α' is the apparent exponent obtained by fitting Equation (22), whereas the exponent α in Equation (28) reflects the actual behavior of the molecule. Dividing Equation (27) by Equation (26) raised to the power 2α, we obtain the relationship

$$\langle R_g^2 \rangle_{Z,i} = k_R^2 M_{W,i}^{2\alpha} \exp[\alpha(2\alpha+1)\sigma_i^2] \tag{29}$$

If the width of each distribution is the same (*i.e.*, σ_i = constant), then the only effect of polydispersity at each elution point is to change the coefficient from k_R^2 to $k_R^2 \cdot \exp[\alpha(2\alpha+1)\sigma_i^2]$. That is, the measured exponent will be the proper value. However, if the width varies systematically with elution volume, then the variation of R_g^2 with mass will be changed. Specifically, if we assume that the width varies in such a way that

$$\exp[\alpha(2\alpha+1)\sigma_i^2] \sim M_{W,i}^{\varepsilon} \tag{30}$$

then the relation in Equation (29) becomes

$$\langle R_g^2 \rangle_{Z,i} = k_R'^2 M_{W,i}^{2\alpha+\varepsilon} \tag{31}$$

A positive value of ε reflects an increasing width with lower elution volume (and thus a larger width for larger masses). This might be caused by lower fractionation efficiency of columns at high molecular weight. This would be expected to have greater effect on hydrodynamically large molecules. A negative value reflects an increasing width with higher elution volume. This might be caused by diffusion, which would more effectively mix hydrodynamically small molecules. A similar calculation relating the weight-average intrinsic viscosity to the weight-average mass results in

$$[\eta]_{W,i} = k'^{2}_{[\eta]} M_{W,i}^{a+\frac{a(a-1)}{\alpha(2\alpha+1)}\varepsilon} \tag{32}$$

where Equation (30) has been used. Therefore, the effect of the supposed systematic variation in polydispersity with elution volume (and thus with mass) is to produce apparent exponents, α' and a', which are related to the actual exponents, α and a, by the relations

$$\begin{aligned} \alpha' &= \alpha + \tfrac{\varepsilon}{2} \\ a' &= a + \frac{a(a-1)}{\alpha(2\alpha+1)}\varepsilon \end{aligned} \tag{33}$$

Note that for $a < 1$, the apparent exponents move in opposite directions ($\alpha' > \alpha$ implies $a' < a$, and vice versa). Equations (33) constitute two equations in three unknowns (the actual exponents α and a, and ε). If we assume that the radius of gyration scales linearly with the hydrodynamic radius, we may impose the condition $a = 3\alpha - 1$, relating a and α. (For impermeable objects such as spheres this relation holds, whereas for open structures, like random coils, it holds in the so-called "non-draining" limit.) With this condition, and for reasonable values of a, the coefficient of ε in the second equation of Equations (33) is slowly varying. We find that minimal error is introduced by replacing it with its average value (–0.20), although results quoted here have used the full system. Using the exponents from Table II and the three equations just developed, we can solve for the three unknowns. These are presented in Table IV. The exponents obtained are far more reasonable. The exponents for PVP are much closer to the expected random coil behavior, the results for T500 are more typical of a branched system, and the HA results are consistent with an expanded random coil. In fact, an electrostatic excluded volume calculation for a molecule with these characteristics produces a R_g exponent of 0.56.[29] The values of ε are also sensible, at least for the unbranched

TABLE IV Exponents α' and a', obtained by fitting R_g vs. molecular weight and η_R ($\equiv[\eta]$) vs. molecular weight, respectively, and the corrected values α and a, obtained by assuming differential fractionation. Also shown is the polydispersity exponent, ε, which quantifies the differential fractionation.

Polymer	α' *apparent* R_g *exponent*	a', *apparent* $[\eta]$ *exponent*	α, *actual* R_g *exponent*	a, *actual* $[\eta]$ *exponent*	ε, *polydispersity exponent*
PVP	0.45 ± 0.015	0.46 ± 0.014	0.48 ± 0.005	0.44 ± 0.016	–0.061 ± 0.031
T500	smallM- 0.56 ± 0.23 largeM- 0.31 ± 0.020	smallM- 0.27 ± 0.015 largeM- 0.12 ± 0.003	smallM- 0.44 ± 0.007 largeM- 0.37 ± 0.002	smallM- 0.33 ± 0.030 largeM- 0.11 ± 0.026	smallM- 0.22 ± 0.046 largeM- –0.11 ± 0.050
HA	0.63 ± 0.039	0.70 ± 0.010	0.57 ± 0.008	0.72 ± 0.048	0.12 ± 0.083

polymers. For HA, a hydrodynamically large molecule, a positive ε suggests a greater effect of incomplete fractionation at high masses, and for PVP, a hydrodynamically small molecule, a negative ε suggests a larger effect of diffusion mixing low mass molecules. For the branched T500, however, the interpretation of ε is not clear. Even so, the assumption of variable widths of mass distributions for different elution volumes does not seem unreasonable.

Observations on "Universal Calibration"

Universal calibration assumes that polymers elute from a column according to hydrodynamic volume.[30,31] That is, it is assumed that the hydrodynamic volume, which is proportional to the product of intrinsic viscosity and molecular weight,

$$V_h \sim [\eta]M \tag{34}$$

is a universal function of elution volume. This suggests that one may infer the mass of a polymer given its elution volume and intrinsic viscosity. Given our data it is possible to test this procedure by constructing "universal calibration" curves of hydrodynamic volume as a function of elution volume. Note we do not use the intrinsic viscosity $[\eta]$ but rather the reduced viscosity η_R, which is measured by the SEC system. It is generally assumed that at the concentrations seen in SEC, the difference between the

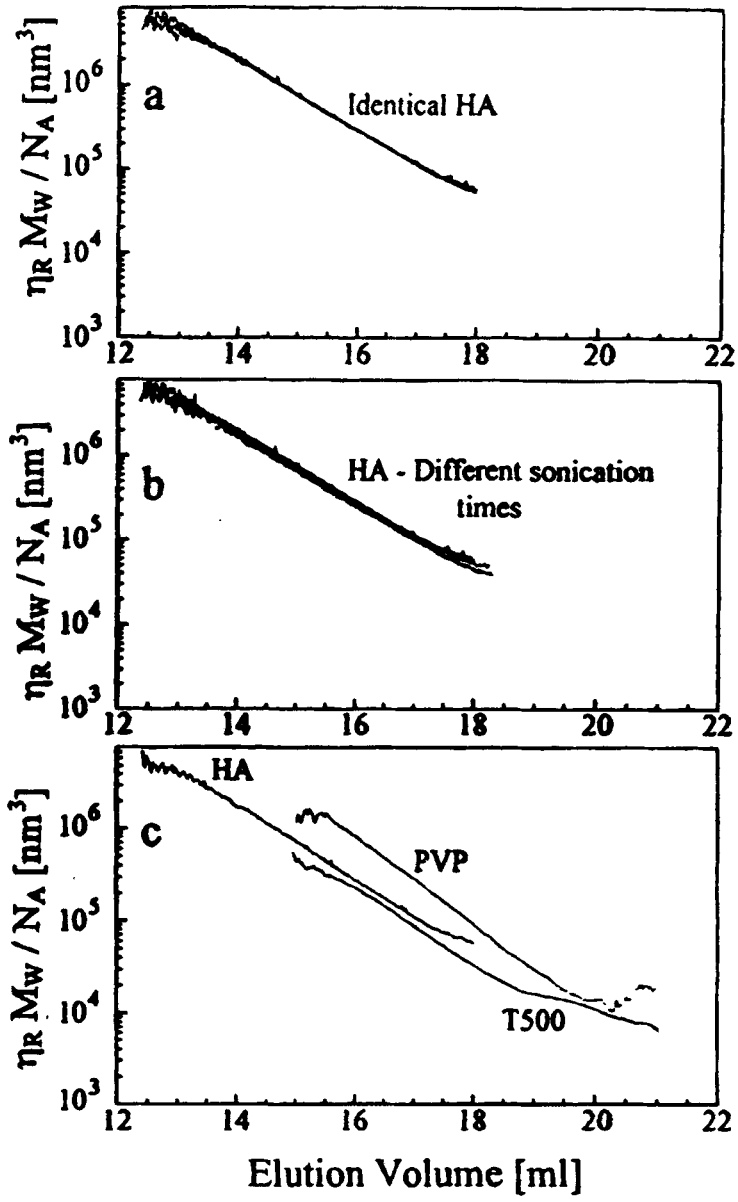

FIGURE 8 "Universal calibration" curves for polymers used in this study. Shown is hydrodynamic volume, expressed as $\eta_R \cdot M_W / N_A$, in nm^3 plotted versus elution volume in mL. a) Five different runs of identical HA over two days, showing the high reproducibility of the experiments. The error in V_h is ±2.6% b) Same data as in a), with additional data from several runs of HA which had been sonicated for varying increments, varying in M_W from 260 kg-mol^{-1} to 330 kg-mol^{-1}. The error in V_h grows to ±10%. c) Three of the polymers used in this study are shown here. For a given elution volume, V_h varies by a factor of more than 2.5. Even if only the polysaccharides, HA and dextran (T500), are considered, the variation in V_h at a given elution volume is ±12.5%.

two viscosities is minimal. In Figure 8a–c, we show such "universal" curves for several of the polymers used in the present investigation. What is plotted is hydrodynamic volume, expressed as

$$V_h = \frac{\eta_R M}{N_A} \tag{35}$$

as a function of the observed elution volume. In Figure 8a, we show five experiments over two days using a single sample of sonicated hyaluronan, whose weight-average molecular weight is 330 kg-mol^{-1}. This shows that the experiments are highly reproducible. The width of the family of curves gives an error in V_h, and thus the inferred molecular weight, of about 2.6%, consistent with the deviation of the viscosities and measured molecular weights used to construct the curve. Figure 8b shows these same five curves, together with four more which show data from the same sample of hyaluronan that had been sonicated for longer periods of time. The weight-average molecular weights of the sonicated hyaluronan vary from 330 to 260 kg-mol^{-1}, a fairly minimal variation. Even so, this family of curves is seen to broaden as compared to those in Figure 8a, such that the error in V_h grows to ±10%. Finally, Figure 8c shows "universal" curves for three polymers: hyaluronan (HA), dextran (T500) and poly(vinyl pyrolidone) (PVP). The three curves are seen to vary by more than a factor of 2.5, rendering the universal calibration procedure virtually useless for determining the mass of polymers not closely related structurally and chemically to the calibration polymers. Even if the vinyl compound, PVP, is excluded and only the two polysaccharides, HA and dextran (T500), are considered, the variation in V_h is over ±12%. Thus, even in very benign circumstances (chemically identical polymers differing only in weight-average molecular weight), "universal calibration" can be expected to give an accuracy of no better than ±10% with the type of columns we have used here.

Failure of universal calibration in aqueous SEC has been reported previously,[25,32–36] and may be due to electrostatic, shear, preferential adsorption and other effects, whereby the mechanism of separation is not purely based on hydrodynamic volume or size exclusion. The failure in this work is actually much smaller than in ref. [25], for example, where the construction of universal calibration curves for different polyelectrolytes with varying solvent ionic strengths produced differences in $\eta_R M$ at each elution point of over two orders of magnitude.

CONCLUSIONS

A systematic and simultaneous comparison has been made of two different viscometer designs coupled with a refractometer and a MALLS detector. Each is seen to have its own set of advantages and disadvantages. First and foremost, an appropriate pump must be chosen in each case. Use of a poor pump, which generates significant pulsations in the mobile phase flow, will seriously degrade the measurements of either viscometer design. In fact, the use of a poor pump with the potentially more accurate bridge viscometer gives worse results than using a superior pump with a single-capillary viscometer. Additionally, the use of a mobile phase that has not been properly degassed introduces significant noise to both viscometers in the form of random pressure excursions.

The two pressure transducers in the bridge viscometer is both an advantage and a disadvantage. The use of a more sensitive transducer to measure the change in viscosity due to the passage of the polymer allows the bridge viscometer to give about an order of magnitude greater precision (~0.01–0.1%) in any given measurement, as compared to the precision of the single-capillary design (~0.1–1%). However, the need to calibrate both transducers, a requirement not present in the single-capillary design, may introduce a systematic error much greater than the observed high precision. Furthermore, the accuracy of the bridge viscometer, as judged by repeated measurements on identical samples, is only about twice that of the single-capillary viscometer. Finally, the significantly greater cost of the bridge viscometer must be mentioned, particularly in that it provides such a marginal benefit in accuracy.

For either viscometer, differential fractionation effects can cause apparent scaling exponents to differ appreciably (10–20%) from their true values. Adding to this the large effect that dead volume uncertainties can have,[25] the scaling exponents reported from such multi-detector SEC systems must be treated with caution.

Acnowledgements

The authors gratefully acknowledge support from the Center for Photoinduced Processes funded by the National Science Foundation and the Louisiana Board of Regents, and the Louisiana Board of Regents University/Industry ties grant RD-B-11.

References

[1] Williams, D. L., Pretus, H. A. and Browder, I. W. (1992). *J. Liq. Chromatogr.*, **15**, 2297.
[2] Wales, M., Marshall, P. A. and Weissberg, S. G. (1952). *J. Polym. Sci.*, **10**, 229.
[3] Senti, F. R., Hellman, N. N., Ludwig, H. H., Babcock, G. E., Tobin, R., Glass, C. A. and Lamberts, B. L. (1955). *J. Polym. Sci.*, **17**, 527.
[4] Lesec, J. and Volet, G. (1990). *J. Appl. Polym. Sci.: Appl. Polym. Symp.*, **45**, 177.
[5] Lesec, J. and Volet, G. (1990). *J. Liq. Chromatogr.*, **13**, 831.
[6] He, X., Lapp, A. and Herz, J. (1988). *Makromol. Chem.*, **189**, 1061.
[7] Schoessler, F., Benoit, H., Grubisic-Gallot, Z., Strazielle, C. and Leibler, L. (1989). *Macromolecules*, **22**, 400.
[8] Kim, S. H., Cotts, P. M. and Volksen, W. (1992). *J. Polym. Sci., Part B: Polym. Phys.*, **30**, 177.
[9] Bauer, J. and Burchard, W. (1993). *Macromolecules*, **22**, 3103.
[10] de Gennes, P.-G. (1979). *Scaling Concepts in Polymer Physics*; (Cornell, Ithaca).
[11] Debye, P. (1946). *J. Chem. Phys.*, **14**, 636.
[12] Lecacheaux, D., Lesec, J. and Quivoron, C. (1982). *J. Appl. Polymer Sci.*, **27**, 4867.
[13] Haney, M. A. (1985). *J. Appl. Polymer Sci.*, **30**, 3023.
[14] Giddings, J. C. (1988). *Chem. Eng. News*, **66**, 34.
[15] Caldwell, K. D. (1988). *Anal. Chim.*, **60**, 959.
[16] Beckett, R. (1987). *Environ. Tech. Lett.*, **8**, 339.
[17] Dos Ramos, J. G. and Silebi, C. A. (1990). *J. Colloid Int. Sci.*, **135**, 165.
[18] Wyatt, P. J. (1993). *Anal. Chim. Acta*, **272**, 1.
[19] Brandrup, J. and Immergut, E. H. (eds.). (1989). *Polymer Handbook, 3rd ed.*; (John Wiley & Sons, New York).
[20] Peterlin, A. (1966). *Pure Appl. Chem.*, **12**, 563.
[21] Podzimek, S. (1994). *J. Appl. Polym. Sci.*, **54**, 91.
[22] Jackson, C. and Barth, H. G. (1994). *Trends Polym. Sci.*, **2**, 203.
[23] Jeng, L., Balke, S. T., Mourey, T. H., Wheeler, L. and Romeo, P. (1993). *J. Appl. Polym. Sci.*, **49**, 1359.
[24] Jeng, L. and Balke, S. T. (1993). *J. Appl. Polym. Sci.*, **49**, 1375.
[25] Reed, W. F. (1995). *Macromol. Chem. Phys.*, **196**, 1539, ibid **197**, 2075 (1996).
[26] Reed, W. F. (1996). *ACS Symp. Series*, **635**, 7.
[27] Zimm, B. H. (1948). *J Chem. Phys.*, **16**, 1093.
[28] Fouissac, E., Milas, M. and Rinaudo, M. in press.
[29] Reed, W. F. (1994). *ACS Symp. Series*, **548**, 297.
[30] Benoit, H., Grubisic, C., Rempp, P., Decker, D. and Zilliox, J. G. (1966). *J. Chim. Phys. Phys.-Chim. Biol.*, **63**, 1506.
[31] Grubisic, Z., Rempp, P. and Benoit, H. (1967). *J. Polym. Sci., Polym. Lett. Ed.*, **5**, 753.
[32] Dubin, P. L. and Principi, J. M. (1989). *Macromolecules*, **22**, 1891.
[33] Dubin, P. L., Edwards, S. L. and Mehta, M. S. (1993). *J. Chromatogr.*, **635**, 51.
[34] Bahary, W. S. and Jilani, M. (1993). *J. Appl. Polym. Sci.*, **48**, 1531.
[35] Rinaudo, M. and Tinland, B. (1991). *J. Appl. Polym. Sci.: Appl. Polym. Symp.*, **48**, 19.
[36] Dubin, P. L., Larter, R. M., Wu, C. J. and Kaplan, J. I. (1990). *J. Phys. Chem.*, **94**, 7243.